Beam Damage Detection Using Synchronisation of Peaks in Instantaneous Frequency and Amplitude of vibration Data

Mohsen Mousavi[a], Damien Holloway*[a], J.C. Olivier[a], Amir H. Gandomi *[b]

[a]*School of Engineering, University of Tasmania, Hobart 7005, Tasmania, Australia*
[b]*Faculty of Engineering and IT, University of Technology Sydney, Ultimo, NSW 2007, Australia*

Abstract

This paper explores the advantages of Variational Mode Decomposition (VMD) in detecting local damage on beam type structures (bridge) subjected to a sprung mass (vehicle). VMD is used to decompose the acceleration time history of the bridge at its midspan into its constitutive intrinsic mode functions (IMFs). The instantaneous frequency (IF) and instantaneous amplitude (IA) of the first IMF show irregularities at the damage position. We demonstrate through computer simulation that VMD is superior for detecting damage when compared to the well-known Empirical Mode Decomposition (EMD) method. A new damage sensitive feature (DSF) is also introduced that considers synchronisation of peaks between the IA and IF signals. The results show that the new DSF can enhance the peak at the damage positions while suppressing peaks at other locations.

Keywords: `Vehicle Bridge Interaction, Variational Mode Decomposition, Moving Mass, Vibration, Damage Detection, SHM of Bridge, Empirical Mode Decomposition`

Email addresses: `Corresponding authors: damien.holloway@utas.edu.au` (Damien Holloway*), `gandomi@uts.edu.au` (Amir H. Gandomi *)

1. Introduction

There are two types of damage that are addressed in the context of the structural health monitoring of bridge structures (simply supported beam model). These are (1) local stiffness reduction, such as open or breathing cracks [1, 2, 3] or bolt looseness [4] which are, more often, modeled as a massless rotational spring with a stiffness equal to the stiffness of the reduced section; and (2) Stiffness reduction of a more extensive area of the beam due to fatigue damage [5]. The latter type of damage is mostly modeled by multiplying the stiffness matrix of the defective element [6] by a scalar constant $1 - \lambda$, where λ is a damage index varying between 0 for a healthy structure and 1 for a totally defective element. Equivalently, in other research, the damage is simply modelled as a reduced cross section [7, 8, 9].

Having categorised the types of damage, there are generally two classes of techniques to locate them on bridges. The first category, which is response-based and therefore baseline-free, has roots in signal processing [10]. These methods often seek a peak at the position of the local damage. To characterise the damage, the signal needs to be decomposed into constructive narrow-banded components using some signal decomposition algorithms such as wavelet transform (WT) [11], empirical mode decomposition (EMD) [12, 2, 13], or variational mode decomposition (VMD) [14]. Other signal-based techniques include those based on machine learning algorithms such as deep-learning [15]. The second category is baseline based damage detection techniques [16], in which one compares the response of the defective structure against the response of the healthy structure to derive information about the damage. This often relies on the finite element (FE) model updating of the intact structure. Both the above classes of techniques have been used to locate either local crack or fatigue damage on beam structures in the literature.

A recent review of bridge structure damage identification methods [17] classifies bridges as beam, truss, arch, cable-stayed or suspension, and within the beam bridge category several techniques are described including acceleration-based time-domain damage index waveform analysis. This paper deals with the first type of damage (crack damage) and introduces an acceleration response-based damage detection technique for local crack damage detection on beam bridge structures. Hence no baseline or FE model of the healthy structure is required for detection purposes.

A commonly used excitation for response-based techniques on bridges is the moving load or mass. It has been shown that the deflection response of the beam when using a small and uniform velocity of the moving load is analogous to the Influence Line (IL) of the beam [18]. As such, a quasi-static moving load can be traversed across the bridge to derive the beam IL. According to the Maxwell-Betti principle of reciprocal deflection, the response at some point A on the beam is equal to the deflection of the beam at each load point when a static force is applied to A. This property has recently been used by Sun et al. [6] to obtain the curvature of the beam. Yang et al. [19] had earlier shown that the curvature of the beam is sensitive to damage and, therefore, can be considered a good damage indicator.

The dynamic component of the response has also been shown to contain useful information about damage. For example, wavelet transformation has been used to separate the dynamic response of the beam for damage detection. He et al. argue that the moving load frequency component of the response of the beam is preferred for damage localisation. Therefore, a multi-scale discrete wavelet transform is used in their paper to separate the moving frequency component from beam frequency component for damage localisation [8].

In terms of innovative signal processing used in response-based techniques, the most significant and widely used recent contribution to the field of structural health monitoring (SHM) is Empirical Mode Decomposition (EMD), first introduced by Huang et al. [20]. This is a technique that interpolates splines between the average of the peaks and troughs and recursively subtracts these curves (known as Intrinsic Mode functions, or IMFs) from the original signal.

A key reason for the effectiveness of EMD is that it preserves the nonlinear response of the bridge to the moving mass at the position of the local damage. These nonlinear effects are known to be of higher frequency and therefore the higher frequency bands of the signal (the first intrinsic mode functions, or IMFs) are more sensitive to the damage [12]. Meredith et al. proposed a technique based on the EMD to detect multiple damage on a simply supported beam subjected to a moving load. However, the effect of the road roughness on damage detection is not considered in their work. Obrien et al. [21] used EMD for drive-by bridge damage detection. Although the effect of the road roughness profile is considered in their paper, a difference in the acceleration signals on healthy and the corresponding damaged structures is used, which must be obtained prior to applying EMD. Therefore, the technique requires a baseline to be available from an experiment conducted on the intact structure. However, He et al. argue that a baseline is not generally useful due to the fact that a small fluctuation of the velocity of the moving mass can bring about a discrepancy of the velocity profile for the moving mass (in the experiments conducted on the intact and damaged beams) [7]. Therefore in this paper we propose a baseline-free method which can localise damage on a simply supported beam subjected to a moving mass considering the road profile effects.

Using different instrumentation such as a switch from the bridge to a passing vehicle to collect indirect measurements for the bridge responses has been demonstrated as a useful technique for bridge damage detection in recent years [1, 22]. Unmanned Aerial Vehicles (UAVs) has also been used as a new technique for bridge inspection recently [23, 24]. More advanced strategy using this new technique has been proposed in [25, 26].

Several authors have used the first (highest frequency) IMF for damage detection. For instance, Roveri et al. [2] exploited the EMD algorithm to detect an open crack on beams using the instantaneous frequency (IF) of the first IMF of the dynamic deflection response of the bridge. In a study conducted by Quek et al., the authors investigated the feasibility of application of the Hilbert-Huang transformation (HHT) in locating any types of anomaly in structures using detected propagating wave signals [27]. Pines et al. applied HHT to study damage in some 1D structures by decomposing recorded time series to extract the phase, and damping information [28]. These extracted data are then used to determine the underlying incident energy propagating through the structure.

Cheraghi et al. introduced novel damage indices using EMD and Fast Fourier Transform (FFT) integration for detecting any change in stiffness of a vibrating pipe. The authors studied the first IMF for extracting information about damage. A finite element simulation is carried out for both the healthy and damaged pipe. The results show that the proposed damage indices are sensitive to the size and location of the damage [29].

In one of the first studies to apply EMD to VBI data with introduced noise in the form of road surface roughness, OBrien et al. apply EMD to decompose the acceleration signal of the beam subjected to a moving load into its component [21]. Then the first IMF is obtained from the decomposed acceleration signal to derive information about damage. OBrien et al. define a damage indicator based on the difference between the signals obtained from the intact and damage structure. It is shown that this subtraction can remove the effects of road profile excitation as well.

However, in most of these EMD-based studies, either no noise is present, or a baseline undamaged structure response is required. Many new advanced signal processing techniques have been developed in recent years which can be exploited to capture the nonlinear part of a time series [30, 31]. The following section briefly describes and compares the HHT and EMD signal processing techniques, outlines their shortcomings, and proposes variational mode decomposition (VMD) as an alternative to EMD. VMD was first introduced in the 2014 paper of Dragomiretskiy and Zosso [30], and has been widely used for fault detection in mechanical and electrical applications (see for example [32, 33]).

The paper presents two key contributions as follows: (1) it demonstrates that VMD can be deployed for damage detection on a simply supported beam subjected to a moving mass, including the presence of the road roughness profile, and is superior to EMD because the decomposition can be better controlled to exclude unwanted features; and (2) the instantaneous frequency and amplitude data obtained from the first IMF of the acceleration signal using VMD may be fused in order to better localise damage, as well as to remove any peaks not related to damage.

2. Signal decomposition techniques

2.1. Hilbert transform

The Hilbert transform was first introduced by David Hilbert (1862–1943) [34]. In modern signal processing approaches, the Hilbert transform is widely used to interpret signals. The basic condition for using the Hilbert transform is *causality* which means that the signal at any time is not dependent on any future events or conditions. It follows that the signal for negative time is zero. The general form of the Hilbert transform of a causal signal $g(t)$ is defined as

$$\hat{g}(t) = \lim_{\epsilon \to 0} \frac{1}{\pi} \int_{|\tau - t| > \epsilon} \frac{g(\tau)}{t - \tau} \, d\tau, \tag{1}$$

where, $\hat{g}(t)$ represents the Hilbert Transform of the signal $g(t)$, and the limit satisfies Cauchy principle value for the integral [35]. It can be shown that the integral of Equation 1 converges and consequently the Hilbert transform is well-defined.

Physically, it is often valuable to define a quantity known as the 'instantaneous frequency' (IF) when dealing with a non-stationary signal. Accordingly, an analytic signal $g_a(t)$ is first defined (see Gabor [36]) in which the real and imaginary parts of Gabor's complex signal are the original signal and its Hilbert transform, respectively. Therefore one may write

$$g_a(t) = g(t) + j\hat{g}(t). \tag{2}$$

The resulting analytical signal $g_a(t)$ can be written using Euler's formula in terms of time-variant 'instantaneous amplitude' (IA) $g_m(t)$ and 'instantaneous phase' $\phi(t)$ as

$$g_a(t) = g_m(t) e^{j\phi(t)}, \tag{3}$$

and $g_m(t)$ and $\phi(t)$ are in turn

$$g_m(t) = \sqrt{g^2(t) + \hat{g}^2(t)}, \tag{4}$$

$$\phi(t) = \tan^{-1}\left(\frac{\hat{g}(t)}{g(t)}\right). \tag{5}$$

Finally, the instantaneous frequency (IF) can be evaluated by differentiating the instantaneous phase with respect to time,

$$\omega(t) = \frac{d\phi(t)}{dt}. \tag{6}$$

According to this definition, instantaneous frequency is well-defined when applied to a mono-component or monotonic signal, which means that at each time the signal is not a combination of a number of different signals. Otherwise, the instantaneous frequency for a multi-component signal is meaningless. However, Huang et al. introduced the Hilbert-Huang Transform (HHT) using an Empirical Mode Decomposition (EMD) method to first separate a multi-component signal into its constructive modes, each of which is mono-component (narrow-banded) [20], before applying the Hilbert Transform. The modes thus obtained are termed Intrinsic Mode Functions (IMFs), and the original signal can be fully reconstructed by combining them. The process through which these modes are obtained is a recursive sifting process, described below.

It is shown that the HHT can be applied to a non-stationary non-linear signal, whereas the FFT by definition assumes an energy signal not suitable to non-stationary signals, while the wavelet transform can be applied to non-stationary linear signals.

2.2. Empirical mode decomposition (EMD)

As mentioned in the previous section, the EMD is an empirical decomposition algorithm first introduced by Huang et al. in order to decompose a non-stationary signal into its oscillation modes or IMFs [20]. Despite the traditional linear modal analysis, IMFs extracted from EMD can be non-stationary, i.e. they can be modulated in both amplitude and frequency. However, in common with linear modal analysis, each IMF is narrow band and approximately involves only one mode of oscillation. Hence, the IMF's characteristics can be summarized as follows:

1. as each IMF is narrow band, it involves only one mode of oscillation;
2. each IMF is modulated in both amplitude and frequency;
3. an IMF can be non-stationary.

Figure 1 shows the flowchart of the basic EMD algorithm applied to an arbitrary signal $X(t)$.

2.3. Shortcomings of EMD and alternative approaches

The EMD algorithm has been shown to be very effective in decomposing non-stationary and nonlinear signals into its components and, therefore, has been employed as an effective method for damage detection and other SHM contexts by many researchers [28, 29, 38, 39, 40].

However, although the HHT is considered a good method for studying non-stationary signals, current implementations exhibit some shortcomings rooted in the use of EMD to decompose the signal [41].

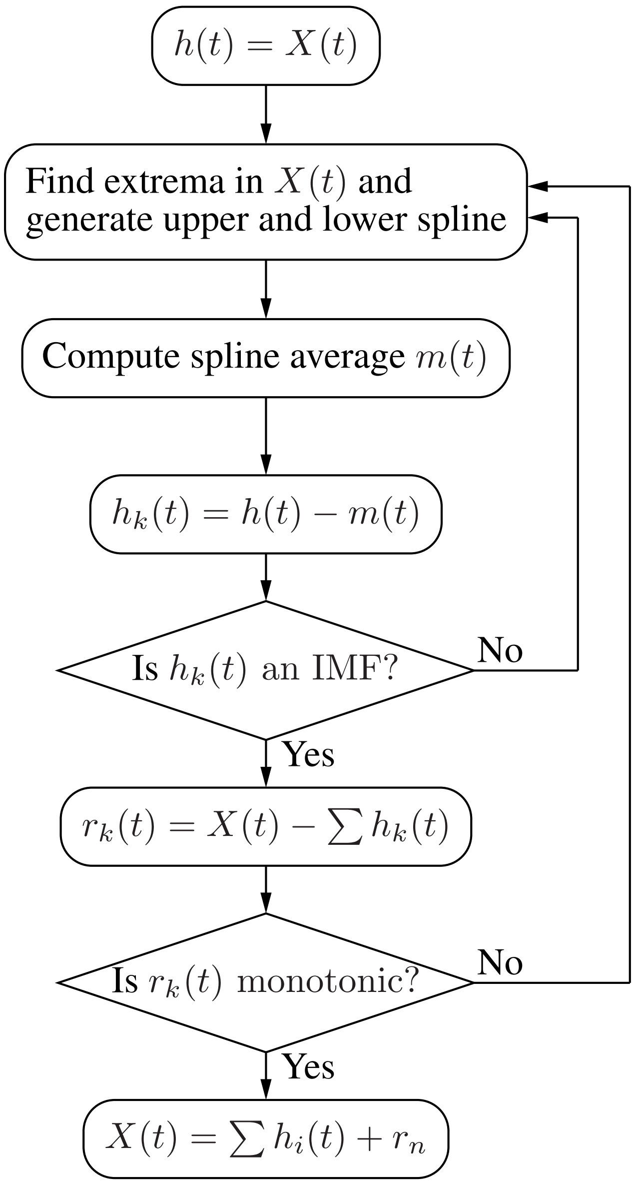

Figure 1: Flowchart for the EMD algorithm [37].

EMD, being an empirical method, sometimes fails to decompose a signal into perfectly narrow-banded components. As a results, the change in instantaneous frequency cannot be detected when the extracted IMF covers a wide-band frequency range. Hence, several modifications have been introduced by researchers to improve the performance of HHT in decomposing a signal into mono-component parts [42, 43].

It has also been argued that EMD shows limitations in terms of sensitivity to noise and sampling [44] and several researchers have introduced new schemes that overcome these limitations. Recently Dragomiretskiy et al. introduced a new method, called variational mode decomposition (VMD), for adaptive decomposition of a signal into its components [30]. The method is a generalization of the classic Wiener filter. Consequently, in contrast to EMD, VMD is entirely non-recursive.

2.4. Variational mode decomposition (VMD)

New signal decomposition methods have been proposed to deal with the shortcomings of EMD. As such, VMD is a newly proposed signal decomposition technique that seeks to decompose a real valued signal $X(t)$ into its components. Since the criteria for a mode to be considered as an IMF slightly changed [45, 46], VMD defines an IMF as an Amplitude-Modulated-Frequency-Modulated (AM-FM) sinusoid with the following additional characteristics:

1. the phase corresponding to an IMF is a non-decreasing function;
2. the envelope of the IMF is non-negative;
3. both the envelope and the instantaneous frequency corresponding to an IMF vary much more slowly than the phase;

As such, the IMF can be written as

$$u_k(t) = A_k(t)\cos(\phi_k(t)) \tag{7}$$

where $A_k(t)$ is the instantaneous amplitude and and $\phi_k(t)$ represents represents the phase. Note that, from Equation 6, $\omega_k(t) = \phi_k'(t)$.

Comparing the new definition of IMF with the original one introduced by Huang et al., it is clear that the new definition is slightly more restrictive. As a result, this forces a mode to have a smaller frequency domain support, complying with the concept of a mono-component signal.

The main algorithm of the VMD method can be found in Dragomiretskiy and Zosso's original paper [30], and the MATLAB code for implementing the algorithm can be found online [47]. Figure 2 shows the general scheme of VMD. In implementing the algorithm, although two further terms are added to the goal function of the optimisation problem, which are (1) a quadratic penalty at finite weight, and (2) a Lagrangian multiplier to strictly enforce the constraint (the reader is referred to the original paper for further details [30]). The former will further guarantee the achievement of convergence in the presence of noise in the signal. As such, three main parameters have to be set in the MATLAB program as follows:

1. a quadratic penalty term (α), higher values of which decrease noise in the decomposed IMFs. However, increasing α also decreases the bandwidth, which decreases the accuracy with which the center frequency of each mode is captured. It is noted that the noise thus eliminated does not appear in the IMFs, hence a version of the original signal with reduced noise is recovered when all the extracted IMFs are summed.
2. the number of modes into which the signal is chosen to be decomposed (k). In contrast to EMD, VMD can decompose the signal into an arbitrary number of IMFs. However, a good decision on the optimum number of IMFs depends on a knowledge of the physics of the studied system. In EMD, the signal is recursively decomposed, therefore the user cannot *a priori* control the number of decomposition steps. This may over-decompose the signal into too many IMFs, especially in the presence of noise, hence individual IMFs may have missing information.
3. the convergence tolerance level (ϵ), which controls the relative error in the reconstructed modes. For small values of ϵ the decomposition is essentially independent of the value chosen.

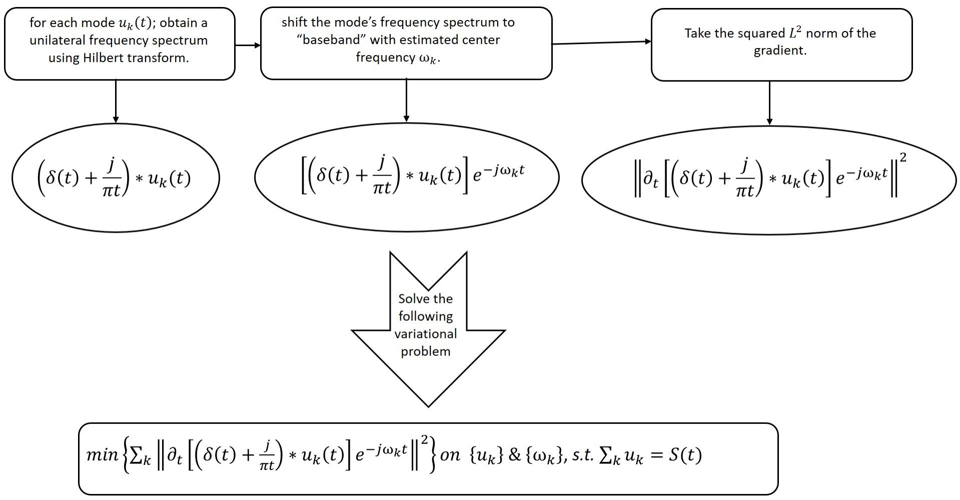

Figure 2: Scheme of the VMD.

3. Vehicle Bridge Interaction (VBI) simulation considering road roughness

In this section, a finite element model of the vehicle bridge interaction is developed, taking into account the road roughness (Figure 3). The example studied in this paper is identical to the one used in [1]. Accordingly, a sprung mass m_v with the stiffness k_v and damping ratio ζ_v is considered to travese the bridge (simply supported beam) at constant velocity, and the interaction between the mass and the bridge is taken into account. Hermite cubic shape function for beam elements are used as follows for finite element modeling,

$$\begin{aligned} N_1 &= 1 - 3\zeta^2 + 2\zeta^3 \\ N_2 &= L_e\left(\zeta - 2\zeta^2 + \zeta^3\right) \\ N_3 &= 3\zeta^2 - 2\zeta^3 \\ N_4 &= L_e\left(-\zeta^2 + \zeta^3\right). \end{aligned} \tag{8}$$

As such, the cubic Hermitian interpolation vector $[N]_c$ evaluated at the contact point is constructed and used in the finite element model of the bridge-vehicle interaction as follows [1],

$$\begin{bmatrix} m_v & 0 \\ 0 & [m_b] \end{bmatrix} \begin{Bmatrix} \ddot{y}_v \\ \{\ddot{q}_b\} \end{Bmatrix} + \begin{bmatrix} c_v & -c_v\{N\}_c^{\tau} \\ -c_v\{N\}_c & [c_b] + c_v\{N\}_c\{N\}_c^{\tau} \end{bmatrix} \begin{Bmatrix} \dot{y}_v \\ \{\dot{q}_b\} \end{Bmatrix}$$
$$+ \begin{bmatrix} k_v & -c_v V\{N'\}_c^{\tau} - k_v\{N\}_c^{\tau} \\ -k_v\{N\}_c & [k_b] + c_v V\{N\}_c\{N'\}_c^{\tau} + k_v\{N\}_c\{N\}_c^{\tau} \end{bmatrix} \begin{Bmatrix} y_v \\ \{q_b\} \end{Bmatrix}$$
$$= \begin{Bmatrix} c_v V r_c' + k_v r_c \\ -c_v V r_c'\{N\}_c - k_v r_c\{N\}_c - m_v g\{N\}_c \end{Bmatrix} \quad (9)$$

where $[m_b]$, $[c_b]$, and $[k_b]$ represent respectively the mass, damping and stiffness matrices of the finite element model of the beam and, as mentioned above, m_v, k_v, and c_v represent respectively the moving mass and its suspension system. Note that in the above equation τ and $'$ represent respectively the transpose of a matrix and derivative with respect to the position, and y_v and $\{q_b\}$ represent respectively, the vertical displacements of the moving mass and the nodal degrees of freedom (vertical translations and rotations) of the VBI elements.

The damping in this equation is modelled as Rayleigh damping, i.e. of the form $[c] = \alpha[m] + \beta[k]$. The Rayleigh constants α and β were set to achieve the target damping ratios specified in Table 1 at the first two natural frequencies, namely 5% and 10% for the beam and suspension respectively.

Finally, r_c denotes an artificial road roughness generated by the following equation from [48], which in turn is based on ISO 8608,

$$r_c(x) = \sum_{i=0}^{N} 2^k \times 10^{-3} \times \sqrt{\Delta n}\left(\frac{n_0}{i\Delta n}\right)\cos\left(2\pi i\Delta n x + \phi_i\right), \quad (10)$$

where the constant $(2^k \times 10^{-3})$ has units $\mathrm{m}^{3/2}$ and Δn has units m^{-1}, hence r_c has units m. The constant scalar k depends on the ISO road profile classification and takes an integer from 3 to 9, corresponding to the profiles from class A to class H (in this paper $k = 3$), and $n_0 = 0.1\ \mathrm{m}^{-1}$. Also in Equation 10, x denotes the variable abscissa on the road with respect to the reference point, ϕ_i is a random phase angle within the range of 0 to 2π with a uniform probabilistic distribution, and $N = L/B$ and $\Delta n = 1/L$, where L is the length of the road profile and B is the wavelength of the shortest spatial component of the roughness profile.

The finite element model of Equation 9 can be solved using Newmark constant average acceleration method in MATLAB with $\beta = 0.25$ and $\gamma = 0.5$. In order to achieve a reasonable initial condition, it is assumed that the mass has been moving over the rough road with a length equal to the length of the bridge L before it arrives at the left hand side of the bridge, and continues moving over the bridge until it reaches the right hand side. Therefore, a road profile for a length of $2L$ is generated and used in simulations.

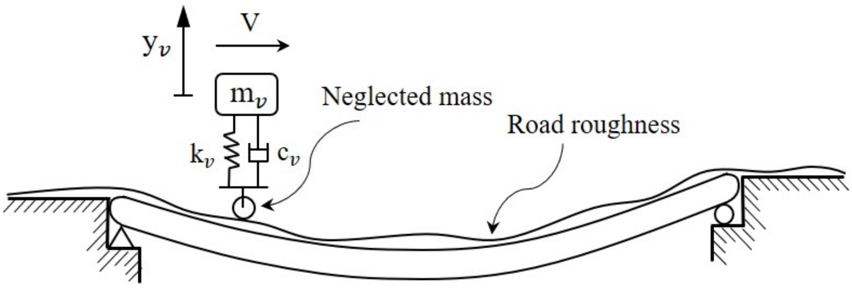

Figure 3: Moving load with suspension system over a bridge with rough surface.

In this paper, the damage is introduced as a zero-length spring located between two standard beam elements, with rotational and translational stiffnesses of k_r and k_t, respectively [49, 50]. As such, the stiffness matrix of the crack element is

$$k_d = \begin{bmatrix} k_t & 0 & -k_t & 0 \\ 0 & k_r & 0 & -k_r \\ -k_t & 0 & k_t & 0 \\ 0 & -k_r & 0 & k_r \end{bmatrix}. \tag{11}$$

In the case that both k_r and k_t are chosen to be sufficiently large, the two section of the beam are fully connected and damage does not exist. Since usually only the loss of the rotational stiffness is considered (representing an open crack) k_t is taken to be a large value of 10^{20} N/m in this paper. In order to calculate k_r, the following formula is used [51],

$$k_r = \left[\frac{2h}{EI} \left(\frac{\alpha}{1-\alpha} \right)^2 \left(5.93 - 19.69\alpha + 37.14\alpha^2 - 35.84\alpha^3 + 13.12\alpha^4\right) \right]^{-1} \tag{12}$$

where the damage parameter $\alpha = 1$ represents no damage ($k_r = \infty$) and $\alpha = 0$ indicates a completely defective section ($k_r = 0$).

The beam is divided into 35 two-dimensional beam elements with rotational and translational degrees of freedom at each node, as shown in Figure 4. Note that the crack elements are not shown in this figure, and that the relevant nodes need to be duplicated.

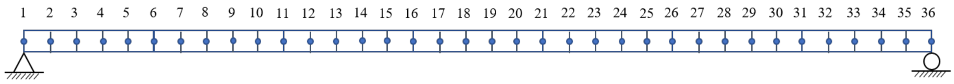

Figure 4: The beam is divided into 35 beam elements bounded by the nodes shown. In addition, to simulate damage, crack elements with stiffness given in Equations 11 and 12 are inserted at nodes 10 only, or 10 and 27, according to the scenarios in Table 2.

4. Numerical Results and Discussions

In this section, the finite element model outlined in the previous section is used to simulate the traverse of a moving mass across a beam with the properties given in Table 1, which give an undamped first natural frequency for the beam alone of 2.67 Hz and an undamped natural frequency suspended mass (in single degree of freedom vibration) of 3.05 Hz. Note that the beam width w does not affect these natural frequencies, it essentially only changes the relativity of the moving mass to the beam mass, so affects the interaction, in particular the overall magnitude of the forcing and response.

Figure 5 shows the road roughness profile used in the simulations generated using Equation 10. Note that, as mentioned above, in order to have realistic and consistent initial conditions when the moving mass enters the bridge, the mass travels one full bridge length before its arrival on the bridge, thus the actual bridge span is from 35 m to 70 m in Figure 5.

Both single and multiple damage scenarios are studied—Table 2 shows the two scenarios considered. While the both methods are computationally efficient in terms of the time required for decomposing the acceleration signal into its IMFs, the aim is to compare the effectiveness of EMD and VMD in detecting these damage scenarios.

4.1. Using EMD for damage detection

It is noted that although OBrien et al. [21] detected damage in a cracked beam by applying EMD to the VBI acceleration data, they needed to subtract the acceleration

Table 1: VBI simulation model constants.

Quantity	nomenculture	Value
Beam modulus of elasticity	E	32.5 GPa
Beam density	ρ	2500 kg/m^3
Beam damping ratio	ζ_b	5%
Beam length	L	35 m
Beam cross-section height	h	2 m
Beam cross-section width	w	1 m
Moving mass magnitude	m_v	1500 kg
Moving mass velocity	V	5 m/s
Suspension stiffness	k_v	550 kN
Suspension damping	ζ_v	10%
Sampling frequency	S_f	1000 Hz

Table 2: Simulated damage scenarios: node positions are shown in Figure 4 (i.e. Nodes 1 and 36 are the ends of the beam) and severity is the quantity $(1 - \alpha)$ in Equation (12).

Damage scenario	Damage position	Damage severity
Single (D1)	Node 10	50%
Multiple (D2)	Nodes 10 & 27	50% & 50%

recorded on the undamaged beam from that of its damaged counterpart to eliminate the road roughness effects. However, more often, the acceleration data from the undamaged beam is not available, and in any case would require the moving mass path and velocity to be absolutely identical in order to experience the same response to road roughness.

In this section therefore, we explore whether an EMD based HHT can detect damage using VBI data from only the damaged beam through studying the instantaneous frequency (IF) or instantaneous amplitude (IA) as defined in Section 2.1. To that end the following steps are followed:

1. EMD is used to decompose the acceleration signal measured at the midspan of the beam into its IMFs.

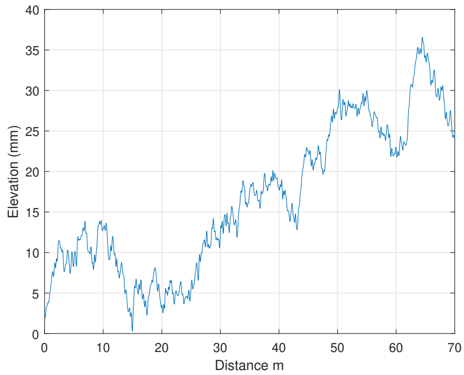

Figure 5: Road roughness profile used in simulations (see Equation 10). The beam spans from 35 m to 70 m.

2. the instantaneous frequency (IF) and instantaneous amplitude (IA) of the first (i.e. highest frequency) IMF are calculated as outlined in Section 2.1. In order to apply Equations 6 in MATLAB, the function `hilbert` is first used to obtain Gabor's complex signal as defined in Equation 2. Then, the command shown in Equation 13 is used to obtain the instantaneous frequency of the constructed analytical signal from the first IMF of the acceleration signal [2, 21],

```
IF = fs/(2*pi)*diff(unwrap(angle(h)));    (13)
```

Figure 6, shows the noise-free simulated acceleration signal at node 19 (the nearest node just to the right of the mid-span) for both damage scenarios. Note that the damage locations correspond to the moving mass positions at normalised times[1] of $9/35 = 0.257$ and $26/35 = 0.743$. As is evident in this figure, the acceleration amplitude in the multiple damage case (Scenario D2) is smaller than in the single damage case (Scenario D1). This is due to the greater relative stiffness reduction of the beam in Scenario D2 compared to Scenario D1.

In the present work, EMD decomposes the acceleration signal into 7 and 8 IMFs for damage scenarios D1 and D2 respectively. Figure 7 shows the first (highest frequency) of these IMFs for each scenario, and their corresponding IF and IA[2]. As can be seen from this figure, there are no obvious features that can be associated

[1] 'Normalised time' indicates the relative position of the load on the beam, where 0 and 1 corresponds respectively to the load entering and exiting the beam span.

[2] In order to exclude end effects at both ends of the signal, the first and last 10 samples of IA

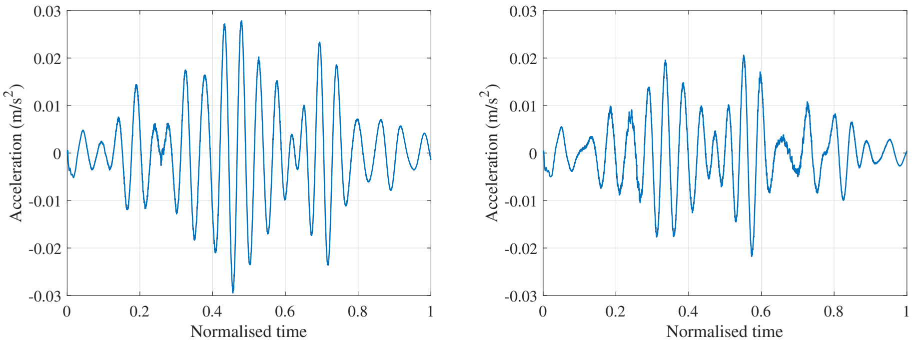

(a) Damage scenario D1 (single crack)

(b) Damage scenario D2 (two cracks)

Figure 6: VBI acceleration data at node 19 for both damage scenario, simulated for a rough road surface but with no added signal noise.

with damage in either the IMF or its IF or IA. The remaining (lower frequency) IMFs were also investigated and similarly found to present no features that could be associated with the cracks.

As such, EMD fails to detect damage on a rough cracked beam subjected to a moving load using data measured only on the damaged beam. In contrast, we show in the next section that VMD is able to detect damage without the baseline state, even with additional noise introduced to the simulated acceleration signals.

4.2. Using VMD for damage detection: noiseless case

A similar procedure to the one discussed in Section 4.1 is followed for damage detection, but using VMD as the decomposition method. However, as discussed in Section 2.4, unlike EMD, the user must make some choices when using VMD. For example, one can specify the number of IMFs into which the signal is decomposed. This is a very important feature of VMD, which helps to manage information in IMFs according to some knowledge about the physics of the system. In the present work, we expect the main responses to be due to the road surface roughness and to the resonant responses of the VBI system, so we choose $k = 3$. Larger values of k lead to duplication of qualitatively similar IMFs, which is not physically meaningful.

and IF are deleted throughout this paper (as recommended in [52, 53]), representing approximately 0.00143 units of normalised time from each end.

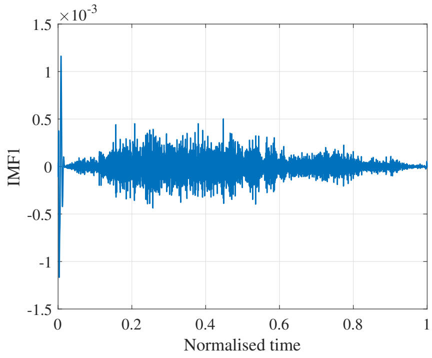

(a)

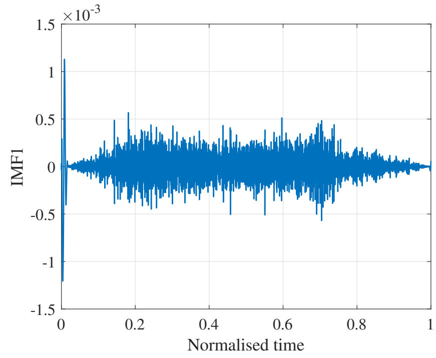

(b)

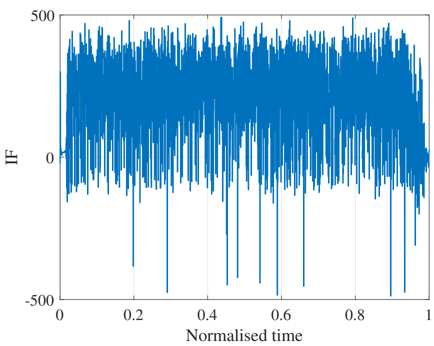

(c)

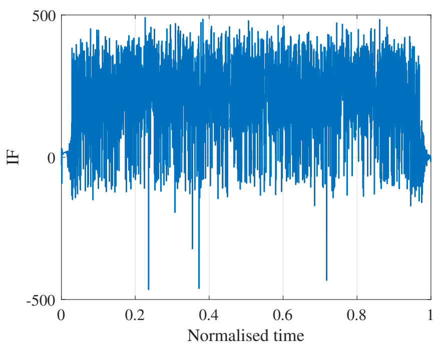

(d)

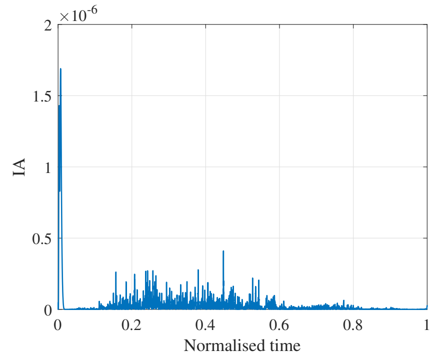

(e)

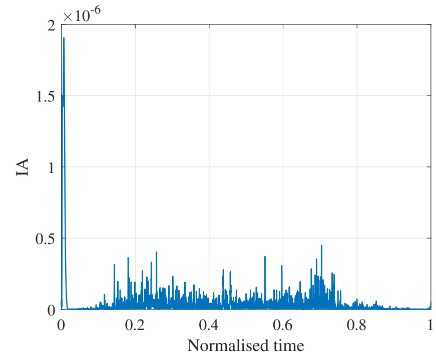

(f)

Figure 7: First (highest frequency) IMFs of VBI mid-span acceleration data, decomposed using EMD, and their corresponding IF and IA for damage scenarios D1 (a, c, and e) and D2 (b, d, and f).

In this section the same acceleration data are used for the damage detection as were used in Section 4.1, i.e. VBI mid-span acceleration for a rough road surface, with no added signal noise. The case of added noise will be investigated in Section 4.2, but for the no added noise case the number of IMFs is set to three ($k = 3$ in the VMD).

Figure 8 shows results using VMD for both damage scenarios. Note that in this case, since there is no noise present in the signal the quadratic penalty term α may be selected as a relative small number of 10000, thereby increasing the accuracy of the center frequency of the modes, while the convergence tolerance level is set to $\epsilon = 10^{-7}$. We explore the use of both the IA and IF of the first (highest frequency)[3] IMFs for damage detection.

Figure 9 shows the IA of the first (highest frequency) IMF for each damage scenario. It is seen that the peaks in the IA plots give a good indication of the location of the damage (at normalised times of 0.26 for D1, and 0.26 and 0.74 for D2). Note that the IA also shows a peak at normalised time of zero—this is not actually damage, but reflects the fact that the beam is simply supported and so may rotate relative to the approaching road, which is the same behaviour as would be produced by a crack.

Next, in Figure 10, we show that the IF may also be used to detect damage. In this case a higher value of α is selected to minimise the high frequency noise-like disturbances caused by the road roughness since the IF requires differentiation of the instantaneous phase angle for its evaluation (Equation 6); we use $\alpha = 90000$ for scenario D1 and 18000 for scenario D2. As such, the IMFs obtained are not the same as those in Figure 8, for which $\alpha = 10000$. As is evident in Figure 10, the large value of α suppresses noise significantly, hence a much lower center frequency is obtained for the first IMF to the extent that this IMF looks much like the second or third IMF of Figure 8.

[3]Note that the numbering sequence of IMFs for EMD is from highest frequency to lowest since they are extracted recursively in that order. However, for VMD they are extracted simultaneously so the numbering is arbitrary. Dragomiretskiy and Zosso number the highest frequency IMF last [30], but to minimise confusion we have kept the same ordering as for EMD.

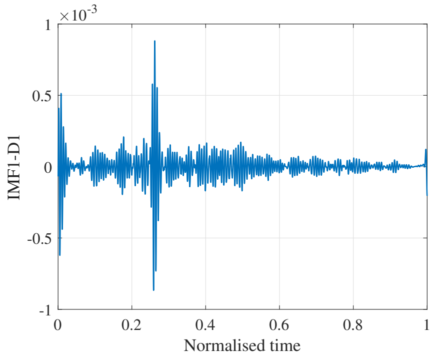

(a)

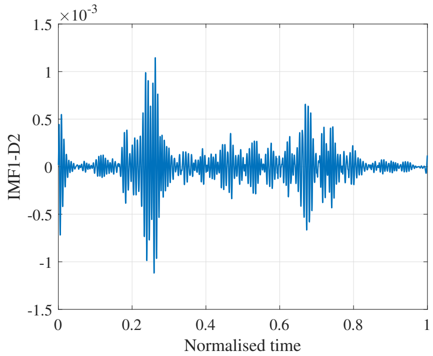

(b)

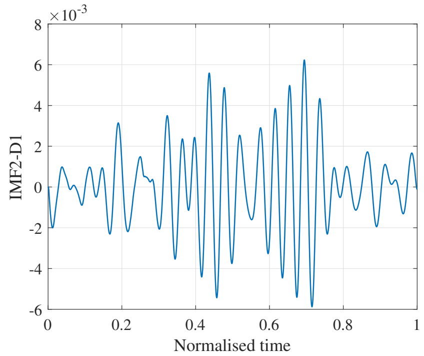

(c)

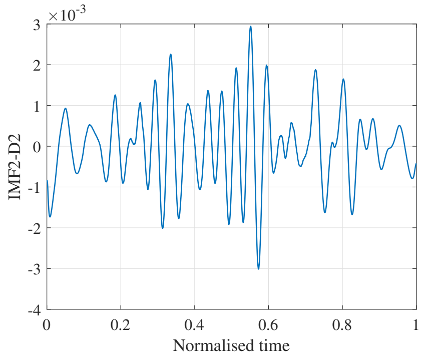

(d)

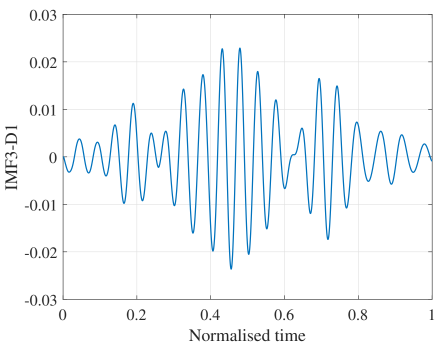

(e)

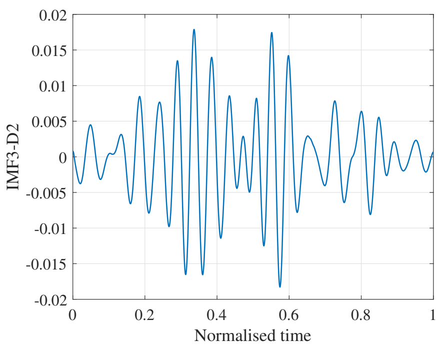

(f)

Figure 8: IMFs of VBI mid-span acceleration of Figure 6, decomposed using VMD with $k = 3$, $\alpha = 10000$ and $\epsilon = 10^{-7}$.

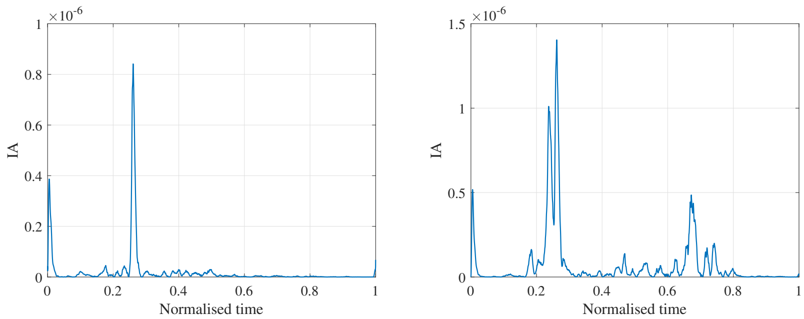

(a) D1 ($\alpha = 10000$) (b) D2 ($\alpha = 10000$)

Figure 9: IA of the first IMFs from VMD of the mid-span acceleration with $k = 3$, $\alpha = 10000$ and $\epsilon = 10^{-7}$. The corresponding IMFs are shown in Figures 8a and 8b respectively. The acceleration signal was simulated for a rough road surface but with no added signal noise.

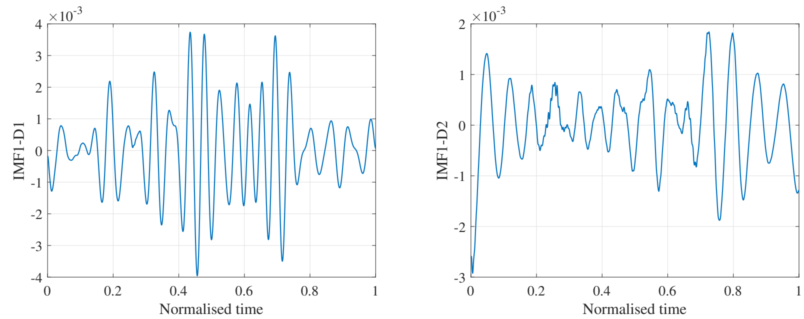

(a) (b)

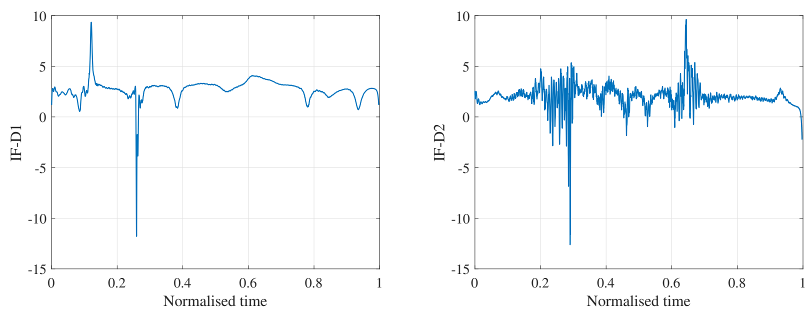

(c) (d)

Figure 10: First (highest average frequency) IMFs and their IFs from VMD of the mid-span VBI acceleration with $k = 3$ and $\epsilon = 10^{-7}$, $\alpha = 90000$ for damage scenario D1 (a and c) and $\alpha = 18000$ for scenario D2 (b and d).

4.3. Using VMD for damage detection: Noisy scenario

In this section, the simulated acceleration data are assumed to be contaminated by noise. To that end, a formula introduce in [18] is used as follows,

$$\hat{\delta} = \delta + \frac{\kappa}{100} n_{\text{noise}}\ \sigma(\delta), \tag{14}$$

where $\hat{\delta}$ represents the vector of noisy measured translational DOF data, δ is the corresponding noise-free vector with standard deviation $\sigma(\delta)$, κ is the noise level in percent (= 10 in the present work) and n_{noise} is a vector with the same length as δ of random independent variables following a standard normal distribution.

In this section, the number of IMFs into which the signal is decomposed is maintained at $k = 3$, as in the previous section. Accordingly, one may expect that the noise must therefore be distributed amongst those three IMFs. However, as discussed above, one needs to minimise the effect of the noise in the resulted IMFs when using IF as a damage locator. This is mainly due to the fact that calculation of the IF requires numerical differentiation of the phase angle, which will amplify any noise.

As mentioned, using a larger value of α will decrease the effect of the noise on each extracted IMF as the effect of Lagrange multiplier in the optimisation goal function is reduced, which can subsequently lead to some of the IMFs being qualitatively similar. In Figure 11, relatively large values of α has been used for both single and double damage scenario. In the case of single damage, since the distortion in the signal is less severe, a very large value of $\alpha = 90000$ may be used to increase the detactability of the damage, while for the case of a more distorted signal from the double damage scenario a value of 29000 for α is sufficient for detecting damage. Again, the damage locations (at normalised times of 0.26 for D1, and 0.26 and 0.74 for D2) are clearly evident in Figure 11.

In contrast to using IF for damage detection, IA does not need such a large value of α to be set due to the fact that there is no differentiation in the formula of IA (Equation 4) and therefore, the effect of noise is not amplified. Figure 12, shows the result obtained from VMD and IA by choosing a considerably smaller value of 9000 for both damage scenarios, and again the single and multiple damage sites are clearly detected.

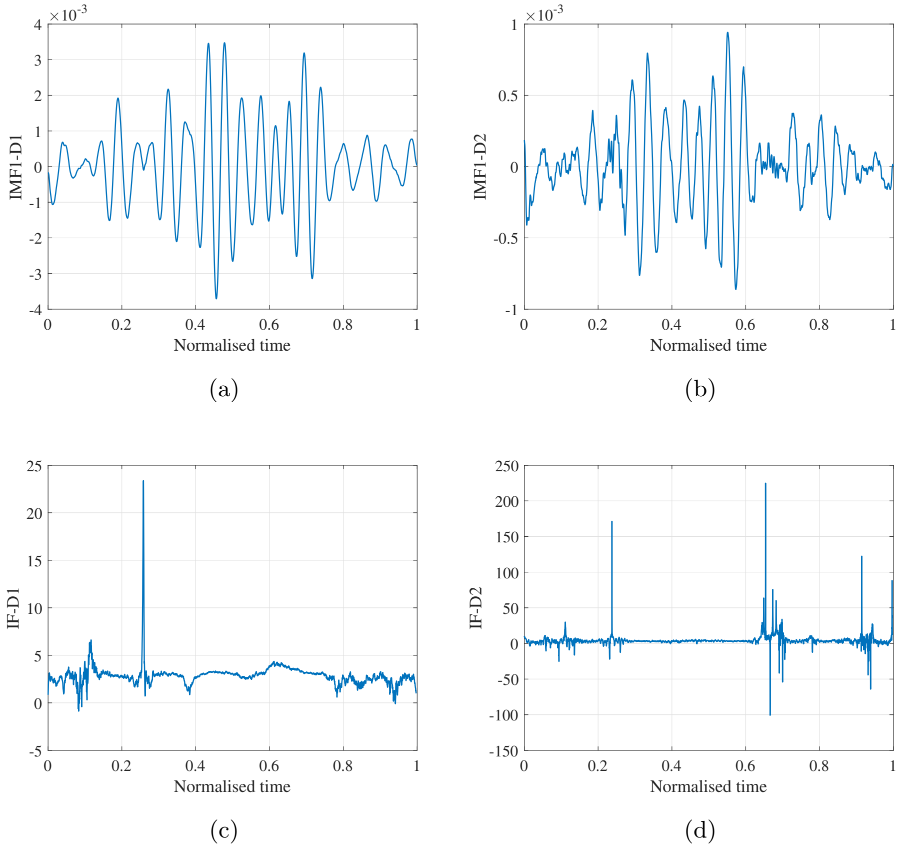

Figure 11: First (highest frequency) IMFs and their IFs from VMD of the mid-span VBI acceleration with $k = 3$ and $\epsilon = 10^{-5}$: damage scenarios D1 (a and c, $\alpha = 90000$) and D2 (b and d, $\alpha = 29,000$) with 10% added noise.

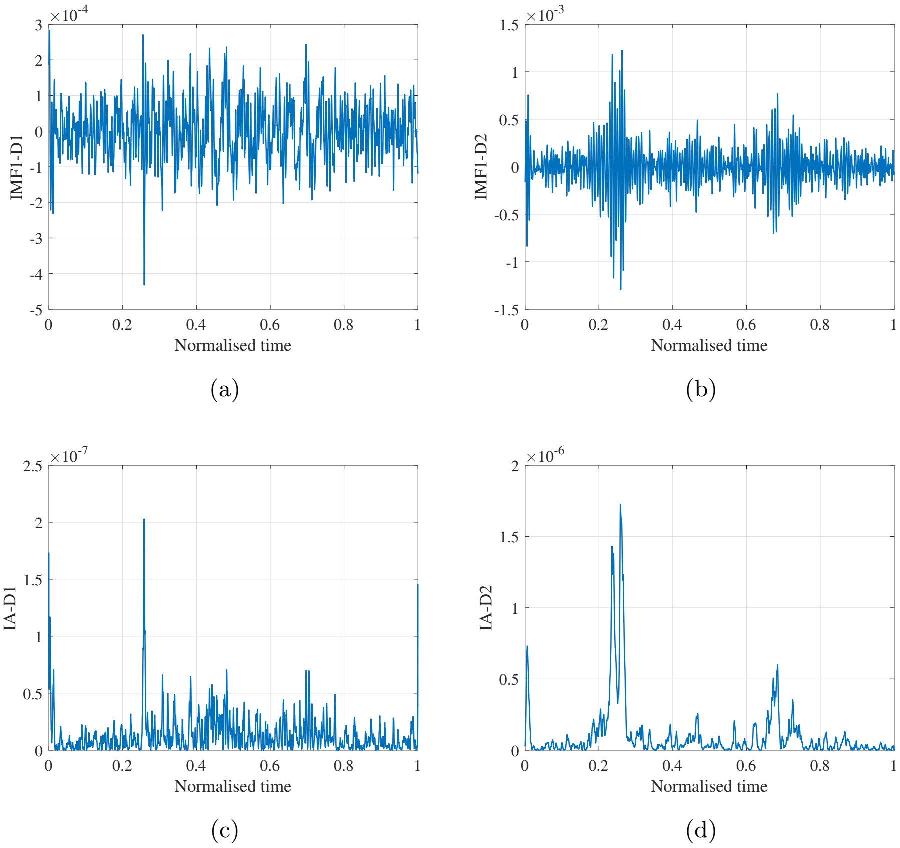

Figure 12: First (highest frequency) IMFs and their IAs from VMD of the mid-span VBI acceleration with $k = 3$ and $\epsilon = 10^{-5}$: damage scenarios D1 (a and b, $\alpha = 9000$) and D2 (c and d, $\alpha = 9000$) with 10% added noise.

4.4. A new damage sensitive feature

In this section a new damage sensitive feature (DSF) based on the synchronisation of peaks in both IA and IF signals is introduced. To that end, we propose multiplication of two signals IA and IF as a new DSF. The intuitive idea behind the proposed DSF comes from the fact that both IF and IA must show a peak at the position of the damage, however, while peaks not associated with damage may occur at other locations in one of the signals it is less likely to be seen in the other one at the same position. Therefore, by multiplying the two signals element-wise, one obtains a new signal with an enhanced peak at the damage position and suppressed peaks at other locations. For instance, it is evident from Figure 10c that the obtained IF also shows a peak not associated with damage at a normalised time (i.e. position) of around 0.11, and several smaller peaks. However, this is not the case for the corresponding IA signal shown in Figure 9a.

As such, the proposed DSF is obtained by first normalising the absolute value of both IA and IF with respect to their maximum values, then multiplying the results as follows,

$$\mathrm{DSF} = \frac{|IA| \odot |IF|}{\max(|IA|) \times \max(|IF|)}\,, \tag{15}$$

where in Equation 15, $\odot$ represents the element-wise multiplication of the absolute value of two signals IA and IF. The DSF obtained thus for the two damage scenarios without signal noise is shown in Figure 13, while Figure 14 shows the DSF for both damage scenarios when IA and IF are obtained from noisy acceleration signal as discussed in Section 4.3. We see now that (excluding end effects) the peaks of the new SDF are confined just to the damage locations.

4.5. Rationale behind the proposed techniques

In this section, the reasons why the obtained results are achieved are discussed. At first, we provide some examples in the literature in which VMD outperforms EMD and related methods, and then we discuss possible reasons reasons why that is the case in the present work.

The superiority of VMD over EMD has been reported in other area of research. For instance, in speech recognition related work, it has been reported that VMD outperforms EMD due to its self-optimisation algorithm and using the Weiner filter

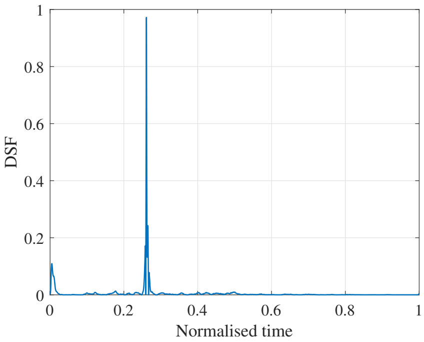

(a) Damage scenario D1 (single crack)

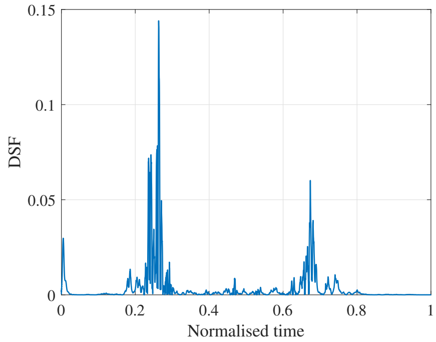

(b) Damage scenario D2 (two cracks)

Figure 13: Obtained DSF for the noiseless first damage scenarios.

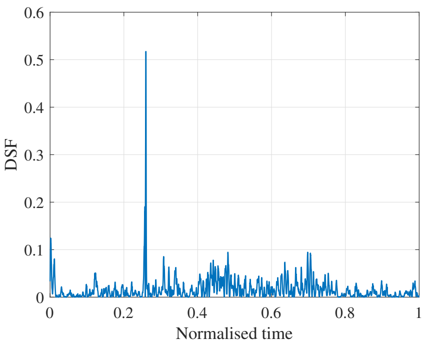

(a) Damage scenario D1 (single crack)

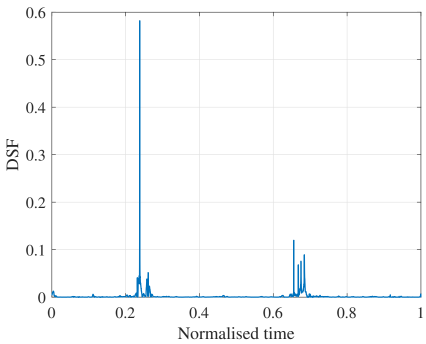

(b) Damage scenario D2 (two cracks)

Figure 14: Obtained DSF for the noisy damage scenarios.

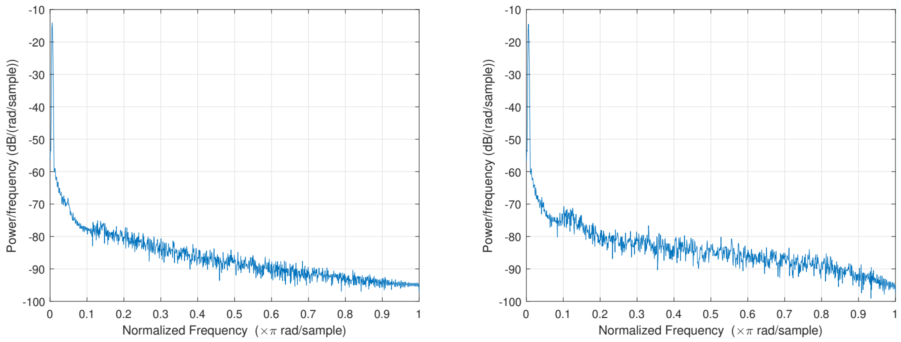

(a) D1

(b) D2

Figure 15: PSD corresponding to the noise-free acceleration signals measured at node 19 for different damage scenarios.

adaptively [54]. In other work related to the forecasting of carbon price using Spiking Neural Networks (SNNs), it has been shown that a VMD-SNN forecasting model outperforms EMD-SNN due to the fact that VMD decomposes the price signal more accurately [55]. The superiority of VMD over modified versions of EMD in damage diagnosis has also been mentioned by others. For instance, it has been reported that a VMD based notch filter approach outperforms the EEMD (Ensemble Empirical Mode Decomposition [56]) algorithm [57].

In terms of the present results, Figure 15 shows the power spectral density (PSD) of the noise-free acceleration signal of the VBI experiment measured at node 19. It is noted that most of the signal energy is concentrated in a low frequency range of 2–4 Hz. EMD and VMD are further used to decompose the signal and the PSD corresponding to each mode is extracted.

Figure 16 shows the one-sided PSD corresponding to the IMFs extracted using EMD (16a and 16b) and VMD (16c and 16d) algorithms, applied to the acceleration signals of the VBI experiment measured at node 19. Note that VMD decomposition has been performed using $\alpha = 90000$ and $\alpha = 29000$ for D1 and D2, respectively, keeping it in line with the previous sections. Neglecting energy levels less than -80 dB, it is apparent from these figures that EMD suffers from the commonly reported mode mixing problem, especially in the few first IMFs (i.e. in the IMFs that show higher energy level for larger normalised frequencies). However, in the case of VMD it can be seen that the energy of the different frequency bands is well separated. This advantage is achieved due to the control over the number of IMFs into which the signal is chosen to be decomposed.

The second phenomenon that is evident from the PSD corresponding to modes of EMD is that the noise is distributed among different modes, which itself interferes with proper separation of modes. In contrast, using VMD, one can deal with this problem by setting α to an appropriate value. As such, VMD can repress the effect of noise in the IMFs better than EMD.

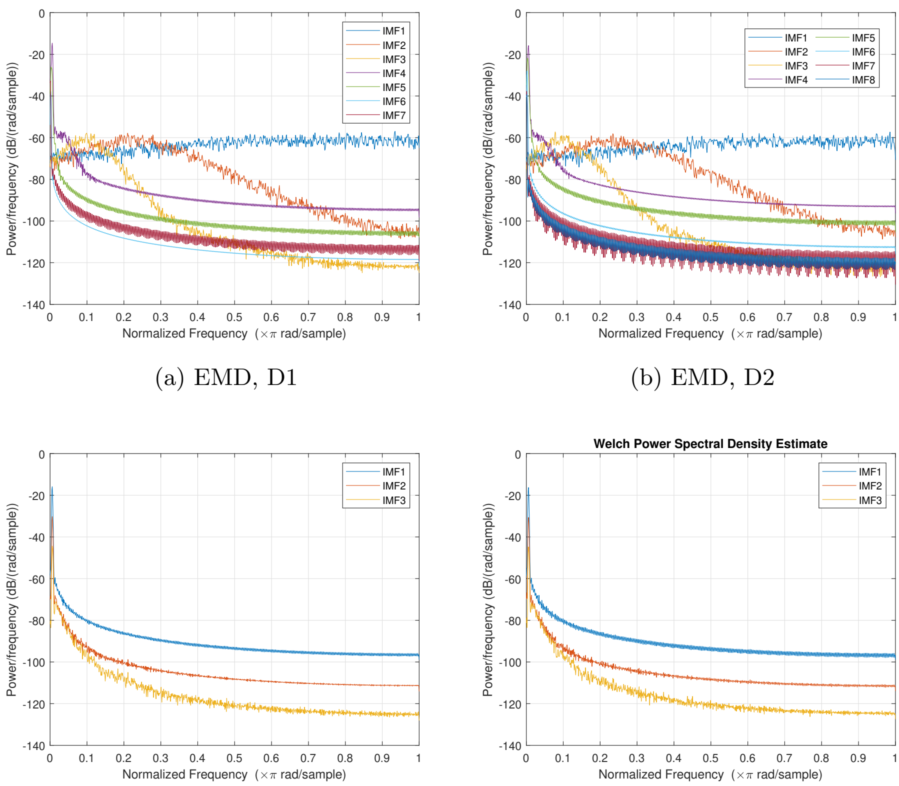

(a) EMD, D1 (b) EMD, D2

(c) VMD, D1 (d) VMD, D2

Figure 16: PSD of the IMFs obtained from VMD and EMD decomposition.

As for the proposed damage sensitive feature, we assume that α can be properly set so that the probability of obtaining a peak at the damage location for both IF and IA equals 1. On the other hand, this probability is significantly less than one in at least one of IF and IA for a peak to appear at a point not associated with damage. Since the IF and IA can be assumed to behave as two independent random variables, due to the fact that two different procedures are followed to calculate IF and IA mathematically, the probability of the the existence of a peak is equal to the multiplication of two probabilities. The probability of detecting spurious peaks is therefore low, corresponding to the probability of such a peak occurring simultaneous in both signals, while the probability remains close to unity for a point genuinely associated with damage.

5. Conclusions

In this paper we compared two main techniques for decomposing the acceleration signal of a VBI model into its IMFs for the purposes of damage detection: EMD and VDM. In accordance with previous studies [21, 12] the first (highest frequency) IMF was then used for damage detection when crack damage was present on the beam. To that end, two main damage detector, i.e. IA and IF, are applied to the derived/extracted IMF to find the damage-induced local change to the signal that was acquired when the vehicle passed over the defective section. The acceleration signal of the VBI model is simulated through a MATLAB code as suggested by [1] and two damage scenarios are considered.

The present study sought to overcome problems that arise when the beam surface roughness is taken into account, which has been shown to interfere with damage detection when using EMD as a decomposition technique. Accordingly, the following novelties were introduced in this study:

1. We showed that, in both damage scenarios, EMD was not able to detect damage using either IF or IA when no baseline from the undamaged beam exist. Some researchers, however, have shown that by subtracting the acceleration data from damaged and undamaged beams, it is possible to detect damage in the presence of road roughness using EMD [21].
2. We showed that VMD can be used successfully to decompose the acceleration signal obtained only on the damaged rough beam subjected to a sprung mass for damage detection. Accordingly two different damage indicators, i.e. IA and IF, can both be used for damage detection without reference to the baseline (undamaged) case.

3. We showed that Both IA and IF are quite successful in detecting damage even in the presence of additional random signal noise.
4. We showed that in the case of using IA for damage detection, one may use a small value of α in the VMD algorithm and, therefore, allow more noise into the decomposed IMF. This is due to the fact that IA will not amplify the effect of noise.
5. We showed that in case of using IF, a relatively large value for α is preferable. This is due to the fact that IF can increase the effect of the noise as its extraction requires differentiation. The large value of α in VMD reduces the effect of noise in the decomposed IMFs, which itself makes the detectability of the damage possible.

Finally a new damage sensitive feature based on synchronisation of peaks between IA and IF derived from the acceleration signal using VMD is proposed. The new DSF shows enhanced peaks at the location of damage while the peaks occuring in other locations are suppressed. While the principle has been demonstrated, further investigation on the application of state-of-the-art signal processing techniques associated with signal synchronisation (for instance based on [58]) could be the subject of future work.

In summary, we conclude that VMD can be used successfully along with IA or IF for damage detection on bridge structures with a surface roughness subjected to a moving vehicle. It is also recommended that both damage indicators IA and IF be used together to increase the reliability and precision in the damage detection using the proposed DSF. However, further study is suggested in order to conclusively establish the applicability of the proposed damage detection strategy of using synchronisation of the IF and IA peaks of the IMF with highest centre frequency obtained using VMD. Furthermore, the applicability to bridges consisting of interconnected beams is also recommended as the subject of future work.

References

References

[1] B. Zhang, Y. Qian, Y. Wu, Y. Yang, An effective means for damage detection of bridges using the contact-point response of a moving test vehicle, Journal of Sound and Vibration 419 (2018) 158–172.

[2] N. Roveri, A. Carcaterra, Damage detection in structures under traveling loads by Hilbert-Huang transform, Mechanical Systems and Signal Processing 28 (2012) 128–144.

[3] K. V. Nguyen, Comparison studies of open and breathing crack detections of a beam-like bridge subjected to a moving vehicle, Engineering Structures 51 (2013) 306–314.

[4] W. Zhang, J. Li, H. Hao, H. Ma, Damage detection in bridge structures under moving loads with phase trajectory change of multi-type vibration measurements, Mechanical Systems and Signal Processing 87 (2017) 410–425.

[5] M. Kurata, J.-H. Kim, J. P. Lynch, K. H. Law, L. W. Salvino, A probabilistic model updating algorithm for fatigue damage detection in aluminum hull structures, in: ASME 2010 Conference on Smart Materials, Adaptive Structures and Intelligent Systems, American Society of Mechanical Engineers, 2010, pp. 741–750.

[6] Z. Sun, T. Nagayama, M. Nishio, Y. Fujino, Investigation on a curvature-based damage detection method using displacement under moving vehicle, Structural Control and Health Monitoring 25 (1) (2018) e2044.

[7] W.-Y. He, W.-X. Ren, S. Zhu, Baseline-free damage localization method for statically determinate beam structures using dual-type response induced by quasi-static moving load, Journal of Sound and Vibration 400 (2017) 58–70.

[8] W.-Y. He, S. Zhu, Moving load-induced response of damaged beam and its application in damage localization, Journal of Vibration and Control 22 (16) (2016) 3601–3617.

[9] W.-Y. He, J. He, W.-X. Ren, Damage localization of beam structures using mode shape extracted from moving vehicle response, Measurement 121 (2018) 276–285.

[10] Y. An, B. Spencer, J. Ou, A test method for damage diagnosis of suspension bridge suspender cables, Computer-Aided Civil and Infrastructure Engineering 30 (10) (2015) 771–784. doi:10.1111/mice.12144.

[11] A. Khorram, F. Bakhtiari-Nejad, M. Rezaeian, Comparison studies between two wavelet based crack detection methods of a beam subjected to a moving load, International Journal of Engineering Science 51 (2012) 204–215.

[12] J. Meredith, A. González, D. Hester, Empirical mode decomposition of the acceleration response of a prismatic beam subject to a moving load to identify multiple damage locations, Shock and Vibration 19 (5) (2012) 845–856.

[13] E. Poskus, G. Rodgers, C. Zhou, J. Chase, Damage identification for hysteretic structures using a mode decomposition method, Computer-Aided Civil and Infrastructure Engineering 33 (2) (2018) 97–109. doi:10.1111/mice.12317.

[14] Y. Li, G. Li, Y. Wei, B. Liu, X. Liang, Health condition identification of planetary gearboxes based on variational mode decomposition and generalized composite multi-scale symbolic dynamic entropy, ISA Transactions 81 (2018) 329–341.

[15] Y. Zhang, Y. Miyamori, S. Mikami, T. Saito, Vibration-based structural state identification by a 1-dimensional convolutional neural network, Computer-Aided Civil and Infrastructure Engineering (2019). doi:10.1111/mice.12447.

[16] Q. Mao, M. Mazzotti, J. DeVitis, J. Braley, C. Young, K. Sjoblom, E. Aktan, F. Moon, I. Bartoli, Structural condition assessment of a bridge pier: A case study using experimental modal analysis and finite element model updating, Structural Control and Health Monitoring 26 (1) (2019) e2273.

[17] Y. An, E. Chatzi, S.-H. Sim, S. Laflamme, B. Blachowski, J. Ou, Recent progress and future trends on damage identification methods for bridge structures, Structural Control and Health Monitoring (2019) e2416.

[18] W.-Y. He, W.-X. Ren, S. Zhu, Damage detection of beam structures using quasi-static moving load induced displacement response, Engineering Structures 145 (2017) 70–82.

[19] Q. Yang, J. Liu, B. Sun, C. Liang, Damage localization for beam structure by moving load, Advances in Mechanical Engineering 9 (3) (2017). doi:10.1177/1687814017695956.

[20] N. E. Huang, Z. Shen, S. R. Long, M. C. Wu, H. H. Shih, Q. Zheng, N.-C. Yen, C. C. Tung, H. H. Liu, The empirical mode decomposition and the Hilbert spectrum for nonlinear and non-stationary time series analysis, Proceedings of the Royal Society of London A: Mathematical, Physical and Engineering Sciences 454 (1998) 903–995. doi:10.1098/rspa.1998.0193.

[21] E. J. OBrien, A. Malekjafarian, A. González, Application of empirical mode decomposition to drive-by bridge damage detection, European Journal of Mechanics-A/Solids 61 (2017) 151–163.

[22] A. ElHattab, N. Uddin, E. OBrien, Drive-by bridge damage detection using non-specialized instrumented vehicle, Bridge Structures 12 (3-4) (2017) 73–84.

[23] D. Erdenebat, D. Waldmann, Application of the DAD method for damage localisation on an existing bridge structure using close-range UAV photogrammetry, Engineering Structures 218 (2020) 110727.

[24] S. Chen, D. F. Laefer, E. Mangina, S. I. Zolanvari, J. Byrne, UAV bridge inspection through evaluated 3d reconstructions, Journal of Bridge Engineering 24 (4) (2019) 05019001.

[25] A. Altan, R. Hacıoğlu, Model predictive control of three-axis gimbal system mounted on UAV for real-time target tracking under external disturbances, Mechanical Systems and Signal Processing 138 (2020) 106548.

[26] A. Altan, R. Hacioğlu, The controller of the camera used in target tracking for unmanned vehicle with model predictive controller, in: 2014 22nd Signal Processing and Communications Applications Conference (SIU), IEEE, 2014, pp. 1686–1689.

[27] S. T. Quek, P. Tua, Q. Wang, Detecting anomalies in beams and plate based on the Hilbert-Huang transform of real signals, Smart Materials and Structures 12 (3) (2003) 447.

[28] D. Pines, L. Salvino, Structural health monitoring using empirical mode decomposition and the Hilbert phase, Journal of Sound and Vibration 294 (1-2) (2006) 97–124.

[29] N. Cheraghi, F. Taheri, A damage index for structural health monitoring based on the empirical mode decomposition, Journal of Mechanics of Materials and Structures 2 (1) (2007) 43–61.

[30] K. Dragomiretskiy, D. Zosso, Variational mode decomposition, IEEE Transactions on Signal Processing 62 (3) (2014) 531–544.

[31] A. Altan, S. Karasu, S. Bekiros, Digital currency forecasting with chaotic metaheuristic bio-inspired signal processing techniques, Chaos, Solitons & Fractals 126 (2019) 325–336.

[32] X. Chen, Y. Yang, Z. Cui, J. Shen, Vibration fault diagnosis of wind turbines based on variational mode decomposition and energy entropy, Energy 174 (2019) 1100–1109.

[33] X. Wang, J. Gao, X. Wei, G. Song, L. Wu, J. Liu, Z. Zeng, M. Kheshti, High impedance fault detection method based on variational mode decomposition and teager–kaiser energy operators for distribution network, IEEE Transactions on Smart Grid 10 (6) (2019) 6041–6054.

[34] I. Muskhelishvili, Nikolaĭ, J. R. M. Radok, Singular integral equations: boundary problems of function theory and their application to mathematical physics, Courier Corporation, 2008.

[35] F. B. Hildebrand, Advanced calculus for engineers, Prentice-Hall, 1949.

[36] D. Gabor, Theory of communication. part 1: The analysis of information, Journal of the Institution of Electrical Engineers-Part III: Radio and Communication Engineering 93 (26) (1946) 429–441.

[37] M. Mousavi, M. S. Taskhiri, D. Holloway, J. Olivier, P. Turner, Feature extraction of wood-hole defects using empirical mode decomposition of ultrasonic signals, NDT & E International (2020) 102282.

[38] Y. Xu, J. Chen, Structural damage detection using empirical mode decomposition: experimental investigation, Journal of Engineering Mechanics 130 (11) (2004) 1279–1288.

[39] J. N. Yang, Y. Lei, S. Lin, N. Huang, Hilbert-Huang based approach for structural damage detection, Journal of Engineering Mechanics 130 (1) (2004) 85–95.

[40] D. Rezaei, F. Taheri, Damage identification in beams using empirical mode decomposition, Structural Health Monitoring 10 (3) (2011) 261–274.

[41] J.-H. Park, H. Lim, N.-H. Myung, Modified Hilbert-Huang transform and its application to measured micro doppler signatures from realistic jet engine models, Progress In Electromagnetics Research 126 (2012) 255–268.

[42] W.-X. Yang, Interpretation of mechanical signals using an improved Hilbert-Huang transform, Mechanical Systems and Signal Processing 22 (5) (2008) 1061–1071.

[43] Z. K. Peng, W. T. Peter, F. L. Chu, An improved Hilbert-Huang transform and its application in vibration signal analysis, Journal of Sound and Vibration 286 (1) (2005) 187–205.

[44] G. Rilling, P. Flandrin, Sampling effects on the empirical mode decomposition, Advances in Adaptive Data Analysis 1 (01) (2009) 43–59.

[45] I. Daubechies, J. Lu, H.-T. Wu, Synchrosqueezed wavelet transforms: An empirical mode decomposition-like tool, Applied and Computational Harmonic Analysis 30 (2) (2011) 243–261.

[46] J. Gilles, Empirical wavelet transform, IEEE Transactions on Signal Processing 61 (16) (2013) 3999–4010.

[47] VMD, Matlab code (2019).
URL https://au.mathworks.com/matlabcentral/fileexchange/44765-variational-mode-decomposition

[48] M. Agostinacchio, D. Ciampa, S. Olita, The vibrations induced by surface irregularities in road pavements—a Matlab® approach, European Transport Research Review 6 (3) (2014) 267–275.

[49] A. Pandey, M. Biswas, M. Samman, Damage detection from changes in curvature mode shapes, Journal of Sound and Vibration 145 (2) (1991) 321–332.

[50] J. Lee, J. Kim, C. B. Yun, J. Yi, J. Shim, Health-monitoring method for bridges under ordinary traffic loadings, Journal of Sound and Vibration 257 (2) (2002) 247–264.

[51] H. Tada, P. Paris, G. Irwin, The analysis of cracks handbook, New York: ASME Press 2 (2000) 1.

[52] D.-C. Lin, Z.-L. Guo, F.-P. An, F.-L. Zeng, Elimination of end effects in empirical mode decomposition by mirror image coupled with support vector regression, Mechanical Systems and Signal Processing 31 (2012) 13–28.

[53] H. Chen, Y. Yan, J. Jiang, Vibration-based damage detection in composite wingbox structures by HHT, Mechanical Systems and Signal Processing 21 (1) (2007) 307–321.

[54] R. Ram, M. N. Mohanty, Comparative analysis of emd and vmd algorithm in speech enhancement, International Journal of Natural Computing Research (IJNCR) 6 (1) (2017) 17–35.

[55] G. Sun, T. Chen, Z. Wei, Y. Sun, H. Zang, S. Chen, A carbon price forecasting model based on variational mode decomposition and spiking neural networks, Energies 9 (1) (2016) 54.

[56] Z. Wu, N. E. Huang, Ensemble empirical mode decomposition: a noise-assisted data analysis method, Advances in adaptive data analysis 1 (01) (2009) 1–41.

[57] A. Soualhi, H. Razik, Electrical Systems 2: From Diagnosis to Prognosis, Chapter 4, John Wiley & Sons, 2020.

[58] R. Biswas, K. Khamaru, K. K. Majumdar, A peak synchronization measure for multiple signals, IEEE Transactions on Signal Processing 62 (17) (2014) 4390–4398.